PROCEEDINGS OF SCIENCE

OMC optical monitoring of sources in the 4th IBIS/ISGRI catalogue

Albert Domingo*
Centro de Astrobiología (INTA-CSIC)
POB 78, 28691 Villanueva de la Cañada, Madrid, Spain
E-mail: albert@cab.inta-csic.es

Julia Alfonso-Garzón
Centro de Astrobiología (INTA-CSIC)
POB 78, 28691 Villanueva de la Cañada, Madrid, Spain
E-mail: julia@cab.inta-csic.es

J. Miguel Mas-Hesse
Centro de Astrobiología (INTA-CSIC)
POB 78, 28691 Villanueva de la Cañada, Madrid, Spain
E-mail: mm@cab.inta-csic.es

The Optical Monitoring Camera (OMC) provides the emission of the optical counterparts of the high energy sources being observed by the *INTEGRAL* instruments. With an aperture of 50 mm and a Johnson V filter, OMC is able to detect optical sources brighter than around $V \approx 17$ within its field of view of $5^\circ \times 5^\circ$, which covers the central part of the Fully Coded Field of View of the gamma-ray instruments. We have cross-correlated *The fourth IBIS/ISGRI soft gamma-ray survey catalogue* with the OMC database, which contains presently photometrical data of more than 60 000 sources, both galactic and extragalactic. In this proceeding we compare the optical and soft gamma-ray emission of the objects detected in both energy ranges, and discuss the distribution of the optical to X-ray spectral index (α_{OX}) values between the different classes of objects.

8th INTEGRAL Workshop "The Restless Gamma-ray Universe" - Integral2010,
September 27-30, 2010
Dublin Ireland

*Speaker.

PoS(INTEGRAL 2010)068

1. Introduction

The Optical Monitoring Camera, OMC [9], observes the optical emission from the prime targets of the gamma-ray instruments on-board the ESA mission *INTEGRAL* [12], the Spectrometer SPI [11] and the Imager IBIS [10], with the support of the JEM-X monitor [8] in the X-ray domain. OMC has the same field of view (FOV) as the fully coded FOV of JEM-X, and it is co-aligned with the central part of the larger fields of view of IBIS and SPI. This combination provides invaluable diagnostic information on the nature and the physics of the sources over a broad wavelength range.

OMC provides photometry in the Johnson V-band (centred at 5500 Å) and it is able to monitor sources from $V \simeq 7$ mag (for brighter sources saturation effects appear) to $V \simeq 17$ mag (limiting magnitude for 3σ source detection). Typical observations are done performing a sequence of different integration times, allowing for photometric uncertainties below 0.1 mag for objects with $V \leq 16$. OMC public data are regularly ingested into the OMC Archive [6] (*http://sdc.cab.inta-csic.es/omc/*) which provides access to the OMC data processed with the OSA software delivered by the INTEGRAL Science Data Center (ISDC [3]). It contains presently photometrical data of more than 60 000 sources, both of galactic and extragalactic origin.

The fourth IBIS/ISGRI soft gamma-ray survey catalogue [2] contains 723 high energy sources detected by IBIS/ISGRI until end of April 2008, in the energy range $17-100$ keV . The scientific data set is based on more than 70 Ms of high-quality observations performed during the first five and a half years of the Core Programme and public observations. It includes both transients and faint persistent objects that can only be revealed with long exposure times.

In this proceeding we compare the optical and soft gamma-ray emission of the objects detected in both energy ranges, cross-correlating the fourth IBIS/ISGRI soft gamma-ray survey catalogue with the OMC archive.

2. OMC optical data

The fourth IBIS/ISGRI soft gamma-ray survey catalogue has been cross-correlated with the OMC Archive by using the source names to avoid confusion. As a result 304 sources out of the 723 have been found in the OMC Archive, having at least one optical observation.

Optical data were extracted from the OMC Archive getting one photometric point per shot. The photometric apertures were centred on the source position, as listed in version 5 of the OMC Input Catalogue [5]. The fluxes and magnitudes were derived from a photometric aperture of 3×3 pixels (1 pixel $= 17.504$ arcsec), slightly circularized i.e. removing $1/4$ pixel from each corner (standard output from OSA). Therefore the computed values include the contributions by any other source inside the photometric aperture. In addition, for some extended sources, this 3×3 aperture does not cover the full object size, but just their central region.

To only include high-quality data, some selection criteria were applied to individual photometric points. Shots were checked against saturation, rejecting those with long exposures for the brightest sources, if necessary. For faint sources, a minimum signal-to-noise ratio of 3 was required, but if long exposure shots were available and not saturated, the shortest shots were only used if the signal-to-noise ratio was greater than 10 to avoid poor quality data. Because some of these sources can show extended structure in the OMC images, anomalous PSF, as well as problems

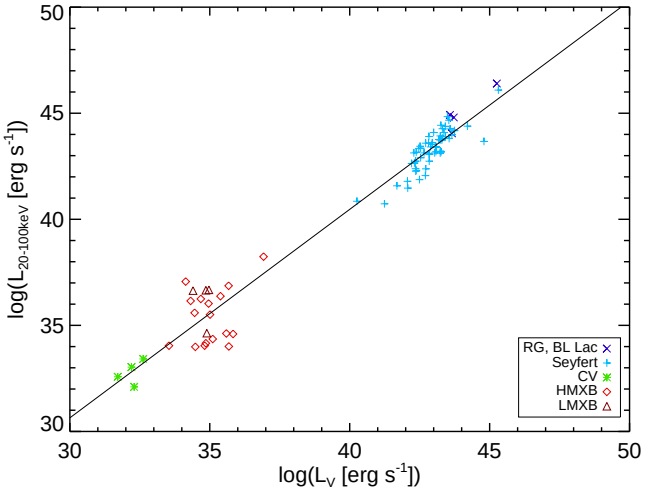

Figure 1: Hard X-ray luminosity L_X versus V-band luminosity L_V. Different types of objects are located along the same dispersion line, over more than 15 decades in luminosity. Part of the dispersion towards higher L_V values originates by the relatively large OMC photometric aperture (52×52 arcsec).

in the centroid determination, were allowed. To avoid contamination by cosmic rays, we excluded those points whose fluxes deviate more than 5 times the standard deviation from the median value of their surrounding points in the light curve. In addition, we rejected those sources with less than 5 OMC photometric points and those reporting only upper limits in the fourth IBIS/ISGRI soft gamma-ray survey catalogue. After applying all these selection criteria our sample contained 220 sources.

As we have already commented the OMC optical fluxes can include contributions by other sources falling inside the photometric aperture used to extract the fluxes. A more detailed analysis revealed that not only some sources are contaminated by others but in some cases the measured flux comes in its totality from other objects falling within the photometric aperture. To avoid the source confusion and only include high-quality OMC data, we rejected from the sample all sources with unknown optical counterpart according to SIMBAD and NED databases. This reduced our sample to 133 sources, from which only 120 can be detected with OMC ($V \lesssim 18$ to be conservative). However the flux we measure for these sources can still include a contribution from other objects within the photometric aperture. We have estimated this contribution by using the GSC 2.3 catalogue [7] and a visual inspection of the optical fields. Finally, our sample is reduced to 90 sources with high-quality OMC optical data. Although we accepted a factor of two in flux as the maximum value of contamination, the 83% of the sample are contaminated by less than 50% in flux and the 67% by less than 10%.

3. Soft gamma-ray and V-band luminosities

Soft gamma/hard X-ray luminosities in the energy band $20-100$ keV were derived by using the fluxes given in the fourth IBIS/ISGRI soft gamma-ray survey catalogue. Source distances were extracted from *The second INTEGRAL AGN catalogue* [1] for most AGN, and SIMBAD and NED

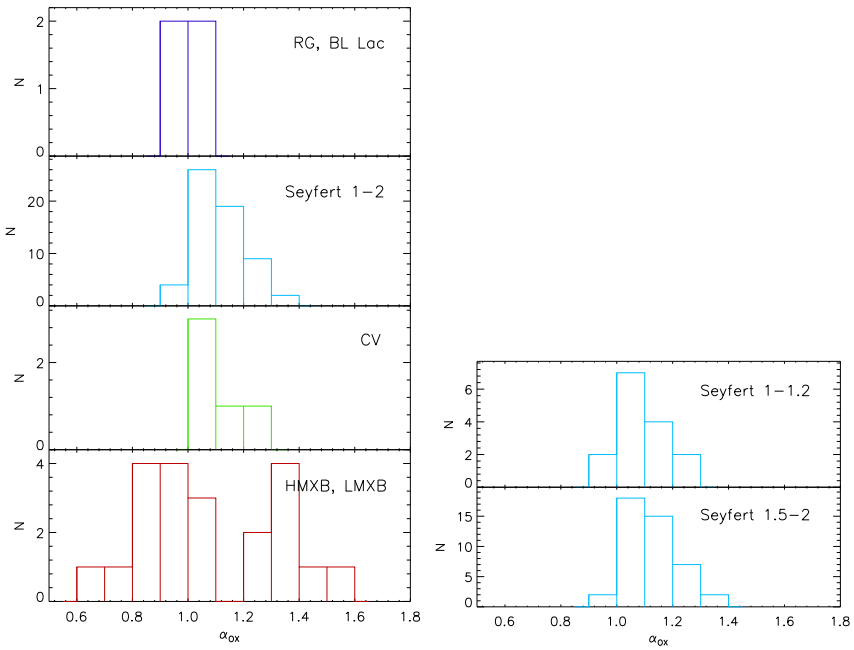

Figure 2: α_{OX} histograms for different types of objects. While the dispersion is large, active galaxies and CVs peak within a relatively narrow range of α_{OX} values around 1.10 ± 0.15. On the other hand, binary systems show a much broader, bimodal distribution.

database for the rest of objects. Distances were available for 87 sources out of 90. To derive the V-band luminosities the median of all good optical measurements was computed for each source.

We show in Fig. 1 the dispersion diagram of L_X vs. L_V , with different symbols for the different classes of objects considered. The source-type classification follows that in the fourth IBIS/ISGRI soft gamma-ray survey catalogue. While the apparent correlation between both luminosities is certainly driven by the distance effect, it is remarkable that the different classes of objects, from cataclysmic stars to AGN, are located on the same correlation line, over more than 15 decades in luminosity.

To further investigate this relation, we computed the histograms of the α_{OX} values for the different kind of objects. This index has the advantage to be distance independent, removing the noise added by the errors in the distance determination. In addition we can use the full sample of 90 sources. The value of α_{OX} is measured as the slope of a power law between the two energy ranges:

$$\alpha_{OX} = -\frac{\log(f_O/f_X)}{\log(\nu_O/\nu_X)}$$

Here, f_O and f_X are the monochromatic fluxes at the frequencies ν_O (at 5500 Å) and ν_X (at 20 keV). To calculate f_X the photon index was taken from *The second INTEGRAL AGN catalogue* [1] when available and fixed to $\Gamma = 2$ for the rest of objects.

We show in Fig. 2 the α_{OX} histograms for the various classes of objects. While the median α_{OX} values are very similar for all sub-samples, their distributions are quite different. The histograms corresponding to radiogalaxies and BL Lac objects would represent mostly the distribution

Name	Type	$f_{20-100\,\mathrm{keV}}$ $[10^{-11}\,\mathrm{erg\,cm^{-2}\,s^{-1}}]$	V [mag]	$\langle\sigma_V\rangle$ [mag]	RMS$/\langle\sigma_V\rangle$	$\log L_{20-100\,\mathrm{keV}}$ $[\mathrm{erg\,s^{-1}}]$	$\log L_V$ $[\mathrm{erg\,s^{-1}}]$	α_{OX}
V709 Cas	CV,IP	5.9	14.00	0.07	1.16	32.58	31.71	1.02
IGR J00370+6122	HMXB,XP,Sg?	0.9	9.65	0.02	2.32	34.01	35.68	1.51
SMC X-1	HMXB,XP	34.3	13.23	0.06	1.01	38.24	36.92	0.94
4U 0115+634	HMXB,XP,T	18.5	15.20	0.23	2.15	36.15	34.32	0.84
RX J0146.9+6121	HMXB,XP,Be,T	1.5	11.42	0.04	1.07	34.04	34.82	1.34
NGC 788	AGN,Sy2	6.0	12.60	0.03	0.96	43.39	43.09	1.15
Mrk 1018	AGN,Sy1.5	1.7	13.84	0.05	0.98	43.81	43.55	1.14
NGC 985	AGN,Sy1	2.4	13.74	0.05	1.06	44.04	43.65	1.12
LS I+61 303	HMXB,?,M	3.0	10.70	0.02	1.18	34.36	35.11	1.33
NGC 1052	AGN,Sy2	1.7	11.38	0.03	0.90	41.93	42.70	1.33
NGC 1068	AGN,Sy2	2.4	9.99	0.02	1.37	43.65	44.80	1.39
NGC 1275	AGN,Sy2	3.8	12.51	0.04	1.03	43.34	43.27	1.17
1H 0323+342	AGN,Sy1	4.0	15.48	0.26	0.75	44.54	43.26	1.02
NGC 1365	AGN,Sy1.8	4.1	11.51	0.05	0.82	42.42	42.72	1.26
EXO 0331+530	HMXB,XP,Be,T	172.3	15.50	0.28	0.62	37.06	34.14	0.63
LEDA 15023	AGN,Sy2	1.9	15.78	0.23	0.90	43.90	42.83	0.98
3C120	AGN,Sy1/BLRG	8.0	14.00	0.05	1.21	44.30	43.31	1.01
UGC 3142	AGN,Sy1	4.9	15.12	0.22	0.59	44.72	43.49	0.96
Ark 120	AGN,Sy1	6.5	12.91	0.04	3.08	44.21	43.74	1.09
1A 0535+262	HMXB,XP,Be,T	8.7	9.00	0.01	10.46	34.62	35.59	1.37
NGC 2110	AGN,Sy2	17.9	12.74	0.04	0.81	43.39	42.53	1.06
Mrk 3	AGN,Sy2	9.5	12.88	0.04	0.93	43.58	42.95	1.09
Mrk 6	AGN,Sy1.5	4.3	13.68	0.06	0.88	43.54	42.94	1.07
IGR J07565-4139	AGN,Sy2	1.4	13.21	0.08	4.14	43.15	43.23	1.16
ESO 209-12	AGN,Sy1.5	2.2	14.60	0.21	0.70	43.91	43.24	1.07
FRL 1146	AGN,Sy1.5	2.1	14.15	0.23	0.61	-	-	1.10
MCG-01-24-012	AGN,Sy2	4.1	14.44	0.12	0.70	43.59	42.72	1.02
NGC 2992	AGN,Sy2	6.5	12.66	0.03	1.01	42.87	42.53	1.12
MCG-05-23-016	AGN,Sy2	14.5	13.12	0.05	0.84	43.36	42.47	1.03
NGC 3227	AGN,Sy1.5	11.3	12.06	0.04	0.37	42.58	42.21	1.12
NGC 3281	AGN,Sy2	5.1	12.67	0.04	1.20	43.11	42.85	1.15
Mrk 421	AGN,BL Lac	37.7	13.03	0.05	2.33	44.86	43.58	0.92
1E 1145.1-6141	HMXB,XP	27.5	12.66	0.15	0.48	36.38	35.38	1.00
2E 1145.5-6155	HMXB,XP	3.4	9.35	0.02	4.57	34.59	35.83	1.42
SWIFT J1200.8+0650	AGN,Sy2	1.7	14.45	0.07	0.81	43.73	43.23	1.09
NGC 4051	AGN,Sy1.5	3.6	12.21	0.05	0.77	41.62	41.69	1.20
NGC 4074	AGN,Sy2	2.2	14.23	0.05	0.80	43.41	42.89	1.09
NGC 4138	AGN,Sy1.9	2.6	11.87	0.05	1.09	41.71	42.06	1.27
NGC 4151	AGN,Sy1.5	30.5	11.49	0.04	4.57	42.86	42.29	1.08
NGC 4395	AGN,Sy1.8	2.1	14.03	0.08	0.65	40.68	40.26	1.09
NGC 4388	AGN,Sy2	24.6	12.22	0.04	1.15	43.59	42.81	1.06
3C 273	AGN,QSO	19.5	12.58	0.04	1.56	46.12	45.31	1.04
V* RT Cru	CV,Symb	5.2	12.15	0.11	1.32	-	-	1.18
LEDA 170194	AGN,Sy2	3.8	14.15	0.06	0.89	44.09	43.37	1.05
NGC 4593	AGN,Sy1	7.1	12.25	0.04	1.33	43.07	42.83	1.15
NGC4748	AGN,NLSy1	1.3	13.26	0.06	1.19	42.74	42.84	1.21
ESO 323-32	AGN,Sy2	1.8	13.11	0.05	0.87	43.02	43.04	1.22
3C 279	AGN,QSO/Blazar	2.2	15.60	0.25	1.82	46.33	45.26	1.02
Mrk 783	AGN,Sy1	2.2	15.33	0.14	1.07	44.40	43.42	1.01
NGC 4941	AGN,Sy2	1.1	12.40	0.03	0.89	40.73	41.24	1.29
ESO 323-77	AGN,Sy1.2	2.6	12.44	0.04	3.18	43.12	43.24	1.25
IGR J13091+1137	AGN,Sy2,XBONG	3.8	13.70	0.05	0.36	43.73	43.18	1.08
MCG-06-30-015	AGN,Sy1.2	4.1	13.23	0.06	0.72	42.75	42.36	1.09
NGC 5252	AGN,Sy1.9	4.8	13.44	0.05	0.89	43.76	43.22	1.09
IC 4329A	AGN,Sy1.2	20.9	13.19	0.05	1.03	44.09	43.00	0.98
NGC 5506	AGN,Sy1.9	14.9	12.93	0.05	0.72	43.21	42.38	1.02
NGC 5548	AGN,Sy1.5	3.0	13.14	0.05	0.70	43.31	43.08	1.15
H 1426+428	AGN,BL Lac	1.8	16.11	0.25	0.61	44.91	43.72	0.96
NGC 5643	AGN,Sy2	1.1	12.17	0.04	0.97	41.47	42.07	1.30
NGC 5995	AGN,Sy2	3.5	13.47	0.07	1.10	43.72	43.29	1.06
Sco X-1	LMXB,Z,M	462.3	12.70	0.03	7.21	36.64	34.40	0.76
IGR J16465-4507	HMXB,XP,SFXT?	1.7	14.43	0.34	0.73	35.51	35.01	1.09
ESO 138-1	AGN,Sy2	2.1	13.53	0.16	9.87	42.58	42.36	1.15
NGC 6221	AGN,Sy1/Sy2	2.1	11.90	0.07	0.41	42.02	42.49	1.29
NGC 6240	AGN,Sy2	5.4	13.06	0.05	1.72	43.87	43.42	1.13
Mrk 501	AGN,BL Lac	4.3	13.21	0.04	1.26	44.06	43.65	1.06
Her X-1	LMXB,XP	86.8	13.42	0.06	4.39	36.66	34.86	0.85
V2400 Oph	CV,IP	3.6	14.47	0.32	0.79	33.03	32.20	1.03
NGC 6300	AGN,Sy2	6.5	11.52	0.05	0.83	42.29	42.38	1.19
XTE J1739-302	HMXB,SFXT	1.7	14.43	0.11	1.82	34.04	33.54	1.09
IGR J17544-2619	HMXB,SFXT	0.8	12.79	0.06	0.67	33.99	34.48	1.28
LS5039	HMXB,NS,M	1.9	11.31	0.05	0.87	34.16	34.86	1.32
ESO 103-35	AGN,Sy2	8.2	13.98	0.07	0.58	43.51	42.51	1.00
3C 390.3	AGN,Sy1	6.1	14.61	0.13	2.15	44.67	43.54	1.00
V1223 Sgr	CV,IP	8.1	13.51	0.11	1.85	33.42	32.62	1.04
XTE J1855-026	HMXB,XP,T	14.7	14.77	0.29	1.35	36.25	34.68	0.89
SS 433	HMXB,M	10.8	14.03	0.09	3.02	35.59	34.46	0.97
NGC 6814	AGN,Sy1.5	5.7	12.42	0.04	0.98	42.53	42.31	1.16
KS 1947+300	HMXB,XP,T	9.9	13.97	0.27	0.45	36.03	34.96	0.99
4U 1954+31	LMXB,NS,Symb	12.4	10.39	0.03	4.58	34.63	34.89	1.24
Cyg X-1	HMXB,BH,M	1392.2	8.90	0.01	7.26	36.87	35.67	0.96
ESO 399-20	AGN,Sy1	1.8	13.96	0.08	0.51	43.47	43.07	1.18

Name	Type	$f_{20-100\,\mathrm{keV}}$ $[10^{-11}\,\mathrm{erg\,cm^{-2}\,s^{-1}}]$	V [mag]	$\langle\sigma_V\rangle$ [mag]	RMS$/\langle\sigma_V\rangle$	$\log L_{20-100\,\mathrm{keV}}$ $[\mathrm{erg\,s^{-1}}]$	$\log L_V$ $[\mathrm{erg\,s^{-1}}]$	α_{OX}
SS Cyg	CV,DN	4.1	11.75	0.03	85.06	32.10	32.30	1.23
Cyg X-2	LMXB,B,Z	22.1	14.69	0.18	1.12	36.68	34.97	0.86
Mrk 520	AGN,Sy1.9	4.1	13.49	0.05	1.18	43.81	43.31	1.09
NGC 7172	AGN,Sy2	7.9	12.66	0.04	0.88	43.11	42.66	1.10
QSO B2251-178	AGN,Sy1	6.7	14.20	0.09	0.85	-	-	1.00
NGC 7465	AGN,Sy2	2.6	12.82	0.03	0.88	42.39	42.35	1.18
NGC 7469	AGN,Sy1	4.5	12.70	0.04	0.78	44.43	44.21	1.14
MCG-02-58-022	AGN,Sy1.5	4.3	14.13	0.06	0.76	44.36	43.59	0.99

Table 1: X-ray flux in the $20-100$ keV energy band, the median V magnitude, the average of error estimates $\langle\sigma_V\rangle$, a variability index RMS$/\langle\sigma_V\rangle$, the X-ray luminosity in the $20-100$ keV energy band, the luminosity in the Johnson V band and α_{OX} values. See text for details.

associated to the active nucleus. The wings towards high α_{OX} values in Seyfert 1–2 galaxies are probably due to the variable contribution of the disc stellar population within the OMC aperture. NGC 1068, the prototypical, obscured Sy2 galaxy, shows the highest value $\alpha_{\mathrm{OX}} = 1.39$. CVs peak at a value very similar to that of active galaxies. The behaviour of α_{OX} for binary sytems is rather different, showing an apparently bimodal distribution which can not be attributed to contamination. Its origin will be discussed in detail in a forthcoming paper [4].

We list finally in Table 1 the X-ray flux in the $20-100$ keV energy band, the median V magnitude, the average of error estimates (1σ level) given by OSA $\langle\sigma_V\rangle$, a variability index RMS$/\langle\sigma_V\rangle$, the X-ray luminosity in the $20-100$ keV energy band, the luminosity in the Johnson V band (centred at 5500 Å, effective width 890 Å) and the α_{OX} of those sources used in this analysis. RMS$/\langle\sigma_V\rangle > 3$ indicates the source has been optically variable within the observation period.

Acknowledgments

The activities related to INTEGRAL-OMC are being funded by the Spanish National Space Programme grant MICINN AYA 2008-03467/ESP.

References

[1] Beckmann, V., Soldi, S., Ricci, C., et al. 2009, A&A, 505, 417

[2] Bird, A.J., Bazzano, A., Bassani, L., et al. 2010, ApJS, 186, 1

[3] Courvoisier, T. J.-L., Walter, R., Beckmann, V., et al. 2003, A&A, 411, L53

[4] Domingo, A., Alfonso-Garzón, J., Mas-Hesse, J.M. 2011, in preparation

[5] Domingo, A., Caballero, M.D., Figueras, F., et al. 2003, A&A, 411, L281

[6] Gutiérrez, R., Solano, E., Domingo, A., García, J. 2004, in Astronomical Society of the Pacific Conference Series, Vol. 314, Astronomical Data Analysis Software and Systems (ADASS) XIII, 153

[7] Lasker, B. M., Lattanzi, M. G., McLean, B. J., et al. 2008, AJ, 136, 735

[8] Lund, N. Budtz-Jørgensen, C. Westergaard, N. J., et al. 2003, A&A, 411, L231

[9] Mas-Hesse, J. M., Giménez, A., Culhane, J. L., et al. 2003, A&A, 411, L261

[10] Ubertini, P., Lebrun, F., Di Cocco, G., et al. 2003, A&A, 411, L131

[11] Vedrenne, G. Roques, J.-P. Schönfelder, V., et al. 2003, A&A, 411, L63

[12] Winkler, C., Courvoisier, T. J.-L., Di Cocco, G., et al. 2003, A&A, 411, L1